HOKKAIDO UNIVERSITY

Title	Photoinduced anisotropic distortion as the electron trapping site of tungsten trioxide by ultrafast W L-1-edge X-ray absorption spectroscopy with full potential multiple scattering calculations
Author(s)	Koide, Akihiro; Uemura, Yohei; Kido, Daiki et al.
Citation	Physical chemistry chemical physics, 22(5), 2615-2621 https://doi.org/10.1039/c9cp01332f
Issue Date	2020-02-07
Doc URL	https://hdl.handle.net/2115/80380
Type	journal article
File Information	ahematite_XFEL_18052019 fdhasc.pdf

Hokkaido University Collection of Scholarly and Academic Papers : HUSCAP

Photoinduced Anisotropic Distortion as the Electron Trapping Site of Tungsten Trioxide by Ultrafast W L1-edge X-ray Absorption Spectroscopy with Full Potential Multiple Scattering Calculations

Akihiro Koide[a,b], Yohei Uemura[a,c]*, Daiki Kido[d], Yuki Wakisaka[d], Satoru Takakusagi[d], Bunsho Ohtani[d], Yasuhiro Niwa[e], Shunsuke Nozawa[e], Kohei Ichiyanagi[e], Ryo Fukaya[e], Shin-ichi Adachi[e], Tetsuo Katayama[f], Tadashi Togashi[f], Shigeki Owada[g], Makina Yabashi[g], Yusaku Yamamoto[h], Misaki Katayama[h], Keisuke Hatada[i], Toshihiko Yokoyama[a]* and Kiyotaka Asakura[d]*

[a.] *Institute for Molecular Science, Myodaiji-cho, Okazaki 444-8585 (Japan). E-mail: yokoyama@ims.ac.jp*
[b.] *CNRS, Institut de Physique de Rennes, University of Rennes, UMR 6251, F-35000 Rennes, France*
[c.] *Inorganic Chemistry and Catalysis, Debye Institute for Nanomaterials Science, Utrecht University, Universiteitslaan 99, 3584 CG Utrecht, The Netherlands. E-mail: yohei.uemura@gmail.com*
[d.] *Institute for Catalysis Hokkaido University, Sapporo 001-0021 (Japan): E-mail: askr@cat.hokudai.ac.jp*
[e.] *Photon Factory, Institute for Materials Structure Sciene, KEK, Tsukuba 305-0801 (Japan)*
[f.] *JASRI, Kouto, Sayo-cho, Hyogo 679-5198 (Japan)*
[g.] *RIKEN SPring-8 Center, Kouto Sayo-cho, Hyogo 679-5148 (Japan)*
[h.] *Department of Applied Chemistry, College of Life Sciences, Ritsumeikan University, Kusatsu, Shiga 525-8577 (Japan)*
[i.] *Department of Physics, University of Toyama, Toyama 930-8555 (Japan)† Footnotes relating to the title and/or authors should appear here.*

Understanding excited state of photocatalysts is significant to improve their activity for water splitting reaction. X-ray absorption fine structure (XAFS) spectroscopy in x-ray free electron lasers (XFEL) is a powerful method to address dynamic changes in electronic states and structures of photocatalysts in excited state in ultrafast short time scales. The ultrafast atomic-scale local structural change in photoexcited WO_3 was observed by W L_1 edge XAFS using an XFEL. An anisotropic local distortion around the W atom could reproduce well the spectral features at a delay time of 100 ps after photoexcitation based on full potential multiple scattering calculations. The distortion involved the movement of W to shrink the shortest W–O bonds and elongate the longest one. The movement of the W atom could be explained by the filling of the d_{xy} and d_{zx} orbitals, which were originally located at the bottom of the conduction band with photoexcited electrons.

Introduction

Photocatalysts and photoelectrodes are key materials for effective solar energy conversion. Metal oxide semiconductors have been researched for decades as photocatalytic materials, and the development of new photocatalytic materials is still of immense research interest. [1-5] Understanding the fundamental properties of photosensitive metal oxides is also important. Among fundamental studies, time-resolved X-ray absorption fine structure (tr-XAFS), which is a relatively new technique, has recently facilitated important achievements in the photoexcited states of photocatalytic materials [6-14]. XAFS is a powerful tool to extract information on the electronic and geometrical structure around a specific element [15, 16] . By combining XAFS with the pump-probe technique, carrier dynamics and local structures have been elucidated in photoexcited state of materials[6-14, 17-24] We have reported the ultrafast photoexcitation of tungsten trioxide (WO_3) nanoparticles sized 50-200 nm, using tr-XAFS at the W L_3 edge, where a core 2p electron is excited to unoccupied d states to monitor the number of photoexcited electrons. [10, 25] WO_3 is a prominent visible-light sensitive photocatalyst and photoelectrode[1-5, 26-31] for the water-splitting reaction, and has been extensively studied.[32, 33] Despite its long developmental history, only few studies have assessed its electronic states and structures during photoexcitation.[26, 34-38] Our results were the first to highlight that the initial photoexcited state to reduce W^{6+} to W^{5+} is transformed into a metastable state with a structure change in 100 ps-200 ps. [7, 25] However, questions have been raised on our interpretation. One is that the structure change time constant (about 100 to 200 ps) is much lower than in other cases. Obara et al. carried out pump-probe XAFS measurements on TiO_2 with a time resolution of 170 fs and detected a structure

change within 300-400 fs. [8] The other is that the local structure around the metastable W atoms remains unclear. Even though the L_3 edge XAFS of W is sensitive to the d orbital vacancy, its spectral shape is too simple to understand subtle structural changes, because it undergoes large life time broadening, and the structure-sensitive multiplet features can hardly be observed, unlike the 3*d* transition metal L_{23} XAFS.[39-44]

In this work, we applied time-resolved L_1-edge X-ray absorption near-edge structure (tr-XANES), which is much more sensitive to the structure and symmetry.[45] The tr-XANES results suggested that an extraordinary structural change was induced after photoexcitation, which could not be explained by a simple lattice expansion. In order to clarify the local structural change, we employed FPMS code based on a full multiple scattering theory [46-48] for XANES simulation. [49] Unlike the conventional multiple scattering code which employs spherically averaged atomic site potentials (i.e., muffin-tin potentials), full potential (or non-muffin-tin) calculations consider all effects of anisotropic potentials on XANES spectra. For instance, the full potential calculations correctly describe the p-d orbital mixing induced by the local centrosymmetric breaking, which cannot be employed in multiple scattering calculations with muffin-tin potentials well. Conventional extension in order to go beyond the spherical potential approximation has been achieved in some all-electron calculation codes by using angular momentum expansion of site effective potentials. [50, 51] However, the outer spheres of such site potentials are truncated with a non-spherical shape. This may imply that the angular momentum expansion of the potentials never be converged in accordance with the Gibbs phenomenon. [52] FPMS code has successfully overcome this convergence issue by using the expansion not for the potential but only for the wave function. [46-48] Consideration of all the asymmetric features of scattering potentials is an essential step to reproduce the L_1 edge XANES precisely, because WO_3 has a distorted O_h symmetry. In this paper, we first present the pump-probe W L_1 edge XANES spectra of WO_3 and determine the structure change by comparing our experimental results to the calculated XANES by FPMS. We discuss the transient structure and the relation to the trapping site, and propose a novel possibility of the trapping site. We also discuss the underlying mechanism for the creation of the metastable state based on a molecular orbital picture.

Experiments and calculations

Time-resolved XAFS experiments

Time-resolved experiments on the picosecond (ps) scale were carried out at the EH2 unit of BL3 [53, 54]in SPring-8 Angstrom Compact Laser (SACLA). A Si(111) channel cut crystal was employed to monochromatize the X-ray pulses, which were focused with Be lenses. [55] All XAFS spectra were measured in the fluorescence mode. The intensity of the elastically scattered X-ray pulses was measured using two photodiodes to obtain the incident X-ray intensity, while the fluorescence X-rays emitted from the sample were measured by another photodiode. A Be thin film was attached to the photodiode to avoid detection of the scattered light of the excitation laser. A chirped-pulse amplified laser was used for sample excitation. The pulse had a duration of approximately 50 fs, wavelength 400 nm, and fluence approximately 200 mJ cm^{-2}. The sample was a suspension of WO_3 nanoparticles with radii between 50 nm and 200 nm and WO_3 concentration of 4 mM. The suspension flowed continuously with a magnetic gear pump to prevent the sample from precipitating. The time resolution of the transient XAFS experiments at SACLA was approximately 500 fs owing to a time jitter. Note that our experimental setup had negligible non-linear effects, as verified by the dependence of the spectral intensity on the pump-pulse intensity (Fig. S1 in Supporting Information).

Time-resolved XAFS experiments on the nanosecond scale were also performed at the NW14A beamline at Photon Factory Advanced Ring (PF-AR) [56], KEK (Proposal No. 2015G541, 2015G542). A fiber laser of wavelength 343 nm, pulse duration 400 fs, and fluence 35 mJ cm^{-2} was employed in order to excite the sample. The repetition rate of the excitation laser was 397 kHz, which is one-half that of the X-ray pulses in PF-AR. The temporal resolution of the experimental setup was approximately 140 ps.

XANES calculations with full potential multiple scattering theory

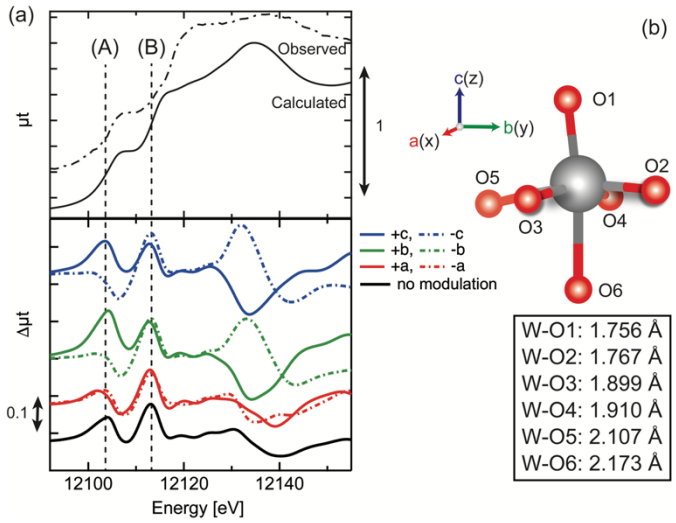


Figure 1. (a) W L_1 edge spectrum of WO_3 (top) and transient XAFS different spectra of photoexcited WO_3 (bottom). The transient spectra at delay times of 0.47 ps and 1.0 ps were measured at SACLA, while that at 150 ps was measured at PF-AR. Error bars were estimated by the variations of the difference signals in the energy region lower than 12100 eV and larger than 12150 eV (b) kinetic traces of W L_1 edge of photoexcited WO_3. A and B correspond to the X-ray absorption at the energy positions in (a) [denoted as (A) and (B)), respectively. (c) kinetic traces of peak A and B in the range between -10 ps and 20 ps. Error bars were estimated by the variations of the laser-off signals.

XAFS spectra were calculated using the FPMS code based on the full potential multiple scattering theory with dipole approximation.[46-48] In the full potential multiple scattering theory, Voronoi cells (or Wigner-Seitz cells) define atomic site regions with no overlap instead of muffin-tin spheres. At the same time, the shape of the potential at each site is exactly considered because the potential at each site is not averaged spherically. For practical calculations, the real part of a Hedin-Lundqvist potential was employed. The broadening parameter *g* was set to 0.2 to include effects of the core-hole life time and the experimental resolution. The maximum value of the partial wave was chosen to be 5. We referred to the reported crystal structure of monoclinic WO_3 with the space group P21/n[29]. The lattice constants in the a, b, and c axes were 7.300, 7.538, and 7.689 Å, respectively. The lattice parameters were $\alpha = \gamma = 90°$ and $\beta = 90.892°$. The modeled WO_3 clusters had a radius of 7 Å. Empty cells, which do not include any atomic center, were employed to fill spaces in the model clusters. These cells were located around each atomic site (W or O site) to form a bcc-like local structure since the Voronoi cell made by surrounding atoms in a bcc structure satisfies the mathematical condition for a free electron propagator, which is employed by FPMS code. The radius of each initial atomic sphere was set to 1.3 Å to enclose each Voronoi cell, which was formed by trimming each initial atomic sphere

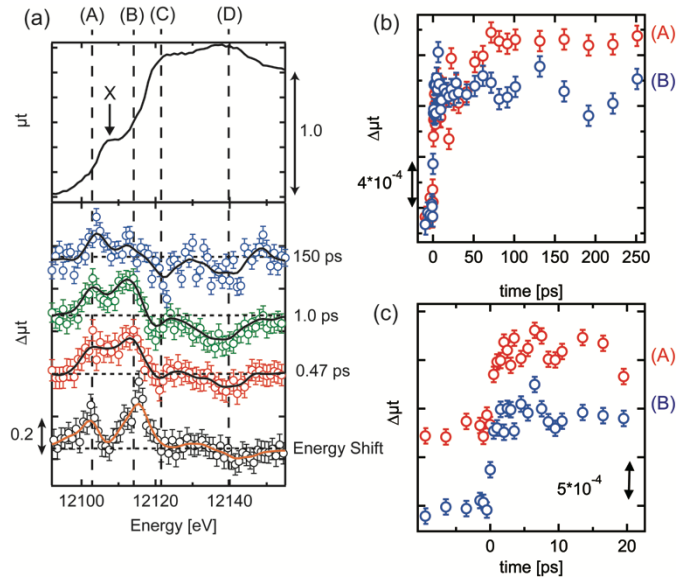


Figure 2. (a) Calculated W L_1 edge spectrum for the ground state (top) and the difference spectra of WO_3 (bottom). The difference spectrum named "no modulation" is the difference between the calculated W L_1 edge spectrum and the one with -1-eV energy shift. The difference spectra with the W movements in the directions ±X (X is a, b or c) were obtained by subtracting the calculated ground-state spectrum from the calculated spectra with the W movements. (b) WO_6 unit and W-O distances of monoclinic WO_3 in the ground state.

in accordance with the Voronoi decomposition. The energy origin for the continuum state was determined by the average of all the surface potentials of Voronoi cells.

Results and Discussions

Time-resolved L_1 edge XAFS

Figure 1(a) shows the W L_1 edge spectrum of WO_3, as well as the transient difference spectra ($\Delta\mu t$ is defined as $\mu t_{excited} - \mu t_{ground}$) at time delays of 0.47, 1.0, and 150 ps. Four significant changes were observed in the difference spectra, at around 12105, 12112, 12120, and 12140 eV, which are denoted as A, B, C, and D, respectively. The last spectrum in Fig. 1(a) (labeled "energy shift")

corresponds to the difference between the observed spectrum in the ground state and the same spectrum shifted by −1 eV. Except for the peak intensities, the peak positions in the energy shift agree with those observed. This negative energy shift is the reflection of the reduction from W^{6+} to W^{5+} that is accompanied by the photoexcitation of the O 2*p* electrons to the W 5*d* orbital, which has been reported in the L_3-edge transient XANES.[25] The pre-edge peak at 12110 eV (denoted as X) indicates the distortion of the symmetric octahedral structure and the degree of the 6*p* orbital mixing. [45] We, therefore, focus on the changes at either side of peak X (positions A and B) because peaks A and B are caused by the shift and intensity change of peak X as shown in Fig. S2. In the figure, the difference spectra between the excited spectrum and the energy shifted ground state spectrum are shown and the intensity peak X gradually increased against the delay times. Reflecting this change of the intensity of the peak X, the transient intensity changes of peaks A and B were different as shown in Fig. 1(b) and Fig. S2.

The intensities of A and B rapidly increased with a delay time of 0 ps. For lower delay times, the intensity of peak B was slightly higher than that of peak A. This could be explained by the edge shift as shown in the last calculated difference spectrum. The intensity of A gradually increased until 150 ps; whereas, the increase in intensity of B was not observed. Finally, the peak intensity of A at 150 ps became greater than that of B as shown in the difference spectrum. The change in the ratio of the difference between the intensity of A and B was caused by the increase in the intensity of peak X as shown in Fig. S2, indicating the gradual local structural change to a maximum of 150 ps. The change of the L_1 difference spectrum agrees well with that observed in our previous work[10, 25] on L_3 edge pump-probe XAFS experiment, where we had concluded that the system reached the metastable state around (140 ± 20 ps.) The continuous change in the peak at A indicated that the population of the transient structure increased to a maximum delay time of 150 ps. The time constant is in the order of 100 ps, which was also in agreement with the time constant for the excited electron to be trapped. [34, 38]

XANES calculations

To analyze the detailed structural change in the metastable WO_3, W L_1-edge XANES spectra were calculated using the FPMS code.[46-48] We focused on the features in the pre-edge region and discussed their changes in the photoexcited state. The difference spectra of the calculated W L_1 XANES were displayed in the bottom of Fig. 2(a). We calculated the spectra with the W atom movement along each crystal axis, defined in Fig. 2(b), show the effects of a local structural change on a W L_1 XANES spectrum. Because the spectral shape of the K and L_1-edge XANES spectra is insensitive to the charge, we shifted the edge of the calculated spectra for the excited state by −1 eV to include the effect of the reduced W ion.

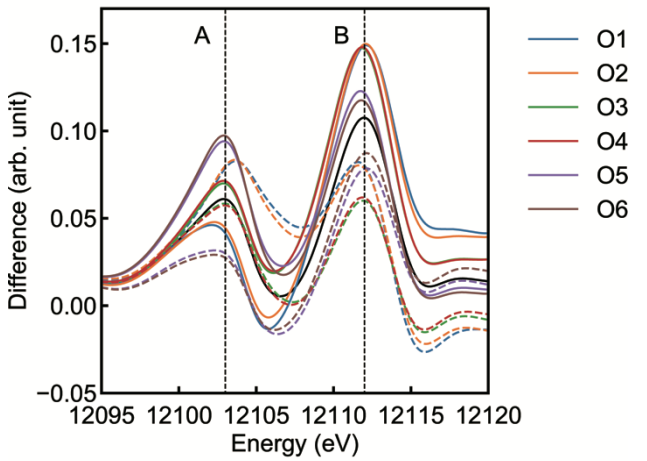


Figure 3. Calculated difference spectra of W L_1 edge XANES for the variation of a W-O bond length. The solid and dash lines show elongation and shrinking of 0.1 Å in the W-O bond length, respectively. Black curve is called “no modulation”.

The difference spectrum termed “no modulation” was calculated by subtracting the unshifted ground state spectrum from the same spectrum shifted by −1 eV. The no modulation spectrum agrees well with the energy shift spectrum in Fig. 1(a), reproducing, in particular, peaks A and B. Thus, we inferred that the initial photoexcited state of WO_3 arose from the electron transfer without a remarkable structure change.

We then calculated the difference spectra between the excited spectrum after shifted W by 0.1 Å in each direction and the -1.0 eV energy shifted ground state spectrum, shown in the lower panel of Fig. 2(a). W was shifted instead of O based on the idea that an ordinary metal oxide is composed of the close packing of anion (O^{2-}) atoms and metal cations are located at the interstitial site. When the W atom was moved toward +c or O1 direction, the intensity of peak A was higher than that of peak B. When the W atom was moved toward +b or O2 direction, the intensity of peak A also increased compared with the no modulation spectrum. Meanwhile, the movements in the opposite direction decreased the intensity of A. In addition to movements parallel to the crystal axes, we found that peak A was also enhanced when W was moved in the diagonal directions when bond lengths between W–O1 or W–O2 were shorter (as shown in Fig. S4). This was rationalized by the increased p-d orbital mixing to enhance the W–O1 or W–O2 bond strength. In other words, peak A became stronger when the distortion of the W local structure increased. To see the relation between the structure of the metastable state and the other WO_3 polymorphs, such as cubic and orthogonal structures, we calculated the XAFS and the difference spectra as shown Fig. S5 in Supporting

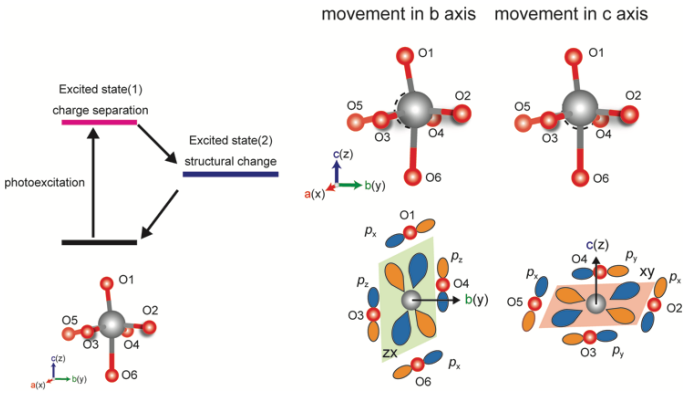


Figure 4. Illustration of the photoexcited process of WO_3

Information. Those structures reduced the pre-edge peak X in the static spectrum and peak A in the difference spectra. Hence, we could not reproduce the tendency of the observed spectra. The metastable state has a distinctive structure that has never been observed before.

When the oxygen was shifted, the same conclusions as shown in Fig. 3 were obtained. The XANES spectra were calculated with shrinking or elongating one W–O bond around the absorbing W atom by 0.1 Å and keeping the other bond lengths constant. The difference spectra were obtained by subtracting the calculated spectrum for the no modulation structure with an energy shift by -1 eV from the spectrum with one bond length changed. The difference of the XANES spectra at 12103 eV increases when the bond length between W and O1 or W and O2 decreases, or that between W and O5 or W and O6 increases. Meanwhile, the difference at 12112 eV decreases when the bond length of W–O1 or W–O2 shrinks. Further, the difference at 12112 eV increases when the bond length of W–O5 or W–O6 elongates. The bond lengths between W–O3 and W–O4 affect the difference at 12112 eV; however, the difference at 12103 eV does not considerably increase.

There have been some reports on photoexcited states of WO_3 in picoseconds, nanoseconds or longer time scales.[34-38] The time scale of photoabsorption process in WO_3 created the conduction electron and then it is trapped for approximately 100–200 ps.[34, 38] The trapped carriers disappeared by the recombination or reaction with the life time in the range of 154–100 μs depending on the particle size, the electron or hole scavengers and the WO_3 nanoparticles' morphology. [34, 35, 37] Our tr-XAFS measurement indicated that the time constant for the transient structure formation was approximately 140 ps, [25] while the metastable state was decayed in approximately 2 ns and connected to the further slower curve. Compared with the previous transient absorption spectra, the delay time of 150 ps corresponds to the formation of the so-called trapping state. In contrast to our results, an electron trapping site, claimed as an oxygen defect site, was located at surface, boundaries of crystallites, or bulk defect in the previous ultrafast x-ray studies [6, 8, 11]. Since the particle size we used in this work was 50–200 nm in diameter and the contribution of the surface could be neglected, the surface defects were less frequently observed. The bulk defect might also be ruled out; the fraction of excited W atoms were estimated to be 30%,[25] and thus, the required O vacancy is 5 %, which is too high to maintain the WO_3 crystalline structure. [57, 58] Therefore, we proposed the trapping site should be the distorted W^{5+} in the normal WO_3 lattice site created 150 ps after the photoabsorption process, where the photo excited electron was stabilized.

The photoexcitation process of WO_3 is summarized in Fig. 4. The W^{5+} state is formed during the initial photoexcitation, which lowers the threshold energy of the W L_1 edge. The initial photoexcited electron state is trapped within 150 ps accompanied by the anisotropic structural changes to form the metastable state. The transient structure of WO_3 gradually recovers to the ground state.

We have proposed the following deformation mechanism to explain the observed structural change in the metastable state of the photoexcited WO_3. The octahedral structure of WO_3 in the ground state is distorted from a regular octahedron by a pseudo Jahn–Teller effect, as shown in Fig. 2(b). [59] Because of this local geometry, the local density of states at the end of the conduction band, *i.e.*, LUMO are mainly composed of W d_{xy} and d_{zx} orbitals (however, not d_{yz}), as shown in Fig. 4, which undergo π antibonding with oxygen atoms at the end of the conduction band. [60] When the electron is excited by the pump-pulse laser, the excited electron occupies the lowest antibonding orbitals d_{xy} or d_{zx}. Consequently, the W–O (2-5, 3-4) (or W–O (1-6,3-4)) bonds are weakened and elongated. This elongation triggers W movement toward O (1) (or O (2)), which has a shorter W–O bond in the ground state. Such anisotropic distortion may stabilize the metastable W^{5+} state and the photoexcited electron is trapped in W^{5+}.

Conclusions

We have carried out W L_1 edge pump-probe experiments on WO_3 and elucidated the local structural change in WO_3 using calculated transient difference spectra for distorted WO_3 structural models. We observed that a W atom anisotropically shifts to make a shorter W–O bond shrink and a longer W–O bond elongate in 150 ps when the initial excited state decays to the metastable state. The mechanism underlying the anisotropic distortion is that the excited electron occupies the end of the conduction band or LUMO states (d_{xy} and d_{zx}) corresponding to the antibonding W–O bonds. We believe that full potential calculations for XANES are quite helpful to understand spectral changes of XAFS caused by an extraordinary structural modification.

Acknowledgements

The XFEL experiments were performed at the BL3 of SACLA with the approval of the Japan Synchrotron Radiation Research Institute (JASRI) (Proposal No. 2017B8020, 2015A8039) This work was financially supported by the JSPS through a Grant-in-Aid for Exploratory Research (No. 26620110), a Grant-in-Aid for Scientific Research (A) (No. 15H02173), a Grant-in-Aid for JSPS Research Fellow (No. 15J07459), Grant for collaborative research in Institute for Catalysis, Hokkaido University (15A1004,18A1005) and polymer membrane fuel cell project from NEDO. This work was partially supported by the ''X-ray Free Electron Laser Priority Strategic Program'' and the ''Photon and Quantum Basic Research Coordinated Development Program'' of MEXT, Japan.

References

1. A. Kafizas, R. Godin and J. R. Durrant, in *Semiconductors and Semimetals*, eds. Z. Mi, L. Wang and C. Jagadish, Elsevier, Editon edn., 2017, vol. 97, pp. 3-46.
2. S. Liu, Z.-R. Tang, Y. Sun, J. C. Colmenares and Y.-J. Xu, *Chem. Soc. Rev.*, 2015, **44**, 5053-5075.
3. K. Maeda and K. Domen, *J. Phys. Chem. Lett.*, 2010, **1**, 2655-2661.
4. R. Abe, *J. Photochem. Photobiol. C: Photochem. Rev.*, 2010, **11**, 179-209.
5. A. Kudo and Y. Miseki, *Chemical Society Reviews*, 2009, **38**, 253-278.
6. T. J. Penfold, J. Szlachetko, F. G. Santomauro, A. Britz, W. Gawelda, G. Doumy, A. M. March, S. H. Southworth, J. Rittmann, R. Abela, M. Chergui and C. J. Milne, *Nat. Commun.*, 2018, **9**, 478.
7. Y. Uemura, D. Kido, A. Koide, Y. Wakisaka, Y. Niwa, S. Nozawa, K. Ichiyanagi, R. Fukaya, S. Adachi, T. Katayama, T. Togashi, S. Owada, M. Yabashi, K. Hatada, A. Iwase, A. Kudo, S. Takakusagi, T. Yokoyamaa and K. Asakura, *Chem. Commun.*, 2017, **53**, 7314-7317.
8. Y. Obara, H. Ito, T. Ito, N. Kurahashi, S. Thürmer, H. Tanaka, T. Katayama, T. Togashi, S. Owada, Y.-I. Yamamoto, S. Karashima, J. Nishitani, M. Yabashi, T. Suzuki and K. Misawa, *Struct. Dyn.*, 2017, **4**, 044033-044033.
9. F. G. Santomauro, A. Lübcke, J. Rittmann, E. Baldini, A. Ferrer, M. Silatani, P. Zimmermann, S. Grübel, J. A. Johnson, S. O. Mariager, P. Beaud, D. Grolimund, C. Borca, G. Ingold, S. L. Johnson and M. Chergui, *Sci. Rep.*, 2015, **5**, 14834.
10. Y. Uemura, H. Uehara, Y. Niwa, S. Nozawa, T. Sato, S. Adachi, B. Ohtani, S. Takakusagi and K. Asakura, *Chem. Lett.*, 2014, **43**, 977-979.
11. M. H. Rittmann‐Frank, C. J. Milne, J. Rittmann, M. Reinhard, T. J. Penfold and M. Chergui, *Angew. Chem. Int. Ed.*, 2014, **53**, 5858-5862.
12. J. E. Katz, X. Zhang, K. Attenkofer, K. W. Chapman, C. Frandsen, P. Zarzycki, K. M. Rosso, R. W. Falcone, G. A. Waychunas and B. Gilbert, *Science*, 2012, **337**, 1200-1203.
13. X. Zhang, G. Smolentsev, J. Guo, K. Attenkofer, C. Kurtz, G. Jennings, J. V. Lockard, A. B. Stickrath and L. X. Chen, *J. Phys. Chem. Lett.*, 2011, **2**, 628-632.
14. J. E. Katz, B. Gilbert, X. Zhang, K. Attenkofer, R. W. Falcone and G. A. Waychunas, *J. Phys. Chem. Lett.*, 2010, **1**, 1372-1376.
15. Y. Iwasawa, K. Asakura and M. Tada, *XAFS Techniques for Catalysts, Nanomaterials, and Surfaces*, Springer International Publishing, 2017.
16. J. A. Van Bokhoven and C. Lamberti, *X‐Ray Absorption and X‐Ray Emission Spectroscopy: Theory and Applications*, John Wiley & Sons, United Kingdom, 2016.
17. M. Ochmann, A. Hussain, I. von Ahnen, A. A. Cordones, K. Hong, J. H. Lee, R. Ma, K. Adamczyk, T. K. Kim, R. W. Schoenlein, O. Vendrell and N. Huse, *J. Am. Chem. Soc.*, 2018, **140**, 6554-6561.
18. B. Dicke, A. Hoffmann, J. Stanek, M. S. Rampp, B. Grimm-Lebsanft, F. Biebl, D. Rukser, B. Maerz, D. Gories, M. Naumova, M. Biednov, G. Neuber, A. Wetzel, S. M. Hofmann, P. Roedig, A. Meents, J. Bielecki, J. Andreasson, K. R. Beyerlein, H. N. Chapman, C. Bressler, W. Zinth, M. Rubhausen and S. Herres-Pawlis, *Natature Chemistry*, 2018, **10**, 355-362.
19. N. A. Miller, A. Deb, R. Alonso-Mori, B. D. Garabato, J. M. Glownia, L. M. Kiefer, J. Koralek, M. Sikorski, K. G. Spears, T. E. Wiley, D. Zhu, P. M. Kozlowski, K. J. Kubarych, J. E. Penner-Hahn and R. J. Sension, *J. Am. Chem. Soc.*, 2017, **139**, 1894-1899.
20. H. T. Lemke, K. S. Kjaer, R. Hartsock, T. B. van Driel, M. Chollet, J. M. Glownia, S. Song, D. Zhu, E. Pace, S. F. Matar, M. M. Nielsen, M. Benfatto, K. J. Gaffney, E. Collet and M. Cammarata, *Nat. Commun.*, 2017, **8**, 15342.
21. M. Chergui and E. Collet, *Chem. Rev.*, 2017, **117**, 11025-11065.
22.M. L. Shelby, P. J. Lestrange, N. E. Jackson, K. Haldrup, M. W. Mara, A. B. Stickrath, D. Zhu, H. T. Lemke, M. Chollet, B. M. Hoffman, X. Li and L. X. Chen, *J. Am. Chem. Soc.*, 2016, **138**, 8752-8764.
23. C. Bressler and M. Chergui, *Annu. Rev. Phys. Chem.*, 2010, **61**, 263-282.
24. C. Bressler and M. Chergui, *Chem. Rev.*, 2004, **104**, 1781-1812.
25. Y. Uemura, D. Kido, Y. Wakisaka, H. Uehara, T. Ohba, Y. Niwa, S. Nozawa, T. Sato, K. Ichiyanagi, R. Fukaya, S.-i. Adachi, T. Katayama, T. Togashi, S. Owada, K. Ogawa, M. Yabashi, K. Hatada, S. Takakusagi, T. Yokoyama, B. Ohtani and K. Asakura, *Angew. Chem. Int. Ed.*, 2016, **55**, 1364-1367.

26. R. Lin, J. Wan, Y. Xiong, K. Wu, W.-c. Cheong, G. Zhou, D. Wang, Q. Peng, C. Chen and Y. Li, *J. Am. Chem. Soc.*, 2018, **140**, 9078-9082.
27. B. Ohtani, *Catalysts*, 2013, **3**, 942-953.
28. Y. P. Xie, G. Liu, L. Yin and H.-M. Cheng, *J. Mater. Chem.*, 2012, **22**, 6746-6751.
29. X. Liu, F. Wang and Q. Wang, *Phys. Chem. Chem. Phys.*, 2012, **14**, 7894-7911.
30. K. Maeda, *J. Photochem. Photobiol. C: Photochem. Rev.*, 2011, **12**, 237-268.
31. P. M. Woodward, A. W. Sleight and T. Vogt, *J. Phys. Chem. Solids*, 1995, **56**, 1305-1315.
32. R. Abe, H. Takami, N. Murakami and B. Ohtani, *J. Am. Chem. Soc.*, 2008, **130**, 7780-7781.
33. R. Abe, T. Takata, H. Sugihara and K. Domen, *Chemical Communications*, 2005, 3829-3831.
34. I. Bedja, S. Hotchandani and P. V. Kamat, *J. Phys. Chem.*, 1993, **97**, 11064-11070.
35. P. S. Patil, P. R. Patil and E. A. Ennaoui, *Thin Solid Films*, 2000, **370**, 38-44.
36. F. M. Pesci, A. J. Cowan, B. D. Alexander, J. R. Durrant and D. R. Klug, *J. Phys. Chem. Lett.*, 2011, **2**, 1900-1903.
37. F. Amano, E. Ishinaga and A. Yamakata, *J. Phys. Chem. C*, 2013, **117**, 22584-22590.
38. K. P. Regan, C. Koenigsmann, S. W. Sheehan, S. J. Konezny and C. A. Schmuttenmaer, *J. Phys. Chem. C*, 2016, **120**, 14926-14933.
39. K. Hong, H. Cho, R. W. Schoenlein, T. K. Kim and N. Huse, *Acc. Chem. Res.*, 2015, **48**, 2957-2966.
40. M. Kubin, M. Guo, M. Ekimova, M. L. Baker, T. Kroll, E. Källman, J. Kern, V. K. Yachandra, J. Yano, E. T. J. Nibbering, M. Lundberg and P. Wernet, *Inorg. Chem.*, 2018, **57**, 5449-5462.
41.M. Kubin, J. Kern, S. Gul, T. Kroll, R. Chatterjee, H. Löchel, F. D. Fuller, R. G. Sierra, W. Quevedo and C. Weniger, *Struct. Dyn.*, 2017, **4**, 054307.
42. M. Kubin, J. Kern, M. Guo, E. Källman, R. Mitzner, V. K. Yachandra, M. Lundberg, J. Yano and P. Wernet, *Phys. Chem. Chem. Phys.*, 2018.
43. B. E. Van Kuiken, H. Cho, K. Hong, M. Khalil, R. W. Schoenlein, T. K. Kim and N. Huse, *J. Phys. Chem. Lett.*, 2016, **7**, 465-470.
44. P. Wernet, K. Kunnus, I. Josefsson, I. Rajkovic, W. Quevedo, M. Beye, S. Schreck, S. Grübel, M. Scholz, D. Nordlund, W. Zhang, R. W. Hartsock, W. F. Schlotter, J. J. Turner, B. Kennedy, F. Hennies, F. M. F. de Groot, K. J. Gaffney, S. Techert, M. Odelius and A. Föhlisch, *Nature*, 2015, **520**, 78.
45. S. Yamazoe, Y. Hitomi, T. Shishido and T. Tanaka, *J. Phys. Chem. C*, 2008, **112**, 6869-6879.
46. K. Hatada, K. Hayakawa, M. Benfatto and C. R. Natoli, *J. Phys.: Condens. Matter*, 2009, **21**, 104206.
47. K. Hatada, K. Hayakawa, M. Benfatto and C. R. Natoli, *J. Phys.: Condens. Matter*, 2010, **22**, 185501.
48. K. Hatada and C. R. Natoli, in *Multiple Scattering Theory for Spectroscopies*, Springer, Editon edn., 2018, pp. 67-91.
49. Y. Joly and S. Grenier, in *X‐Ray Absorption and X‐Ray Emission Spectroscopy*, eds. J. A. Van Bokhoven and C. Lamberti, John Wiley & Sons, United Kingdom, Editon edn., 2016.
50. T. Huhne, C. Zecha, H. Ebert, P. H. Dederichs and R. Zeller, *Phys. Rev. B*, 1998, **58**, 10236-10247.
51. P. Blaha, K. Schwarz, P. Sorantin and S. B. Trickey, *Comput. Phys. Commun.*, 1990, **59**, 399-415.
52. in *Electron Scattering in Solid Matter*, eds. J. Zabloudil, R. Hammerling, P. Weinberger and L. Szunyogh, Springer, Berlin, Editon edn., 2005, vol. 147, pp. 45-56.
53. K. Tono, T. Togashi, Y. Inubushi, T. Sato, T. Katayama, K. Ogawa, H. Ohashi, H. Kimura, S. Takahashi, K. Takeshita, H. Tomizawa, S. Goto, T. Ishikawa and M. Yabashi, *New J. Phys.*, 2013, **15**, 083035.
54. T. Ishikawa, H. Aoyagi, T. Asaka, Y. Asano, N. Azumi, T. Bizen, H. Ego, K. Fukami, T. Fukui, Y. Furukawa, S. Goto, H. Hanaki, T. Hara, T. Hasegawa, T. Hatsui, A. Higashiya, T. Hirono, N. Hosoda, M. Ishii, T. Inagaki, Y. Inubushi, T. Itoga, Y. Joti, M. Kago, T. Kameshima, H. Kimura, Y. Kirihara, A. Kiyomichi, T. Kobayashi, C. Kondo, T. Kudo, H. Maesaka, X. M. Maréchal, T. Masuda, S. Matsubara, T. Matsumoto, T. Matsushita, S. Matsui, M. Nagasono, N. Nariyama, H. Ohashi, T. Ohata, T. Ohshima, S. Ono, Y. Otake, C. Saji, T. Sakurai, T. Sato, K. Sawada, T. Seike, K. Shirasawa, T. Sugimoto, S. Suzuki, S. Takahashi, H. Takebe, K. Takeshita, K. Tamasaku, H. Tanaka, R. Tanaka, T. Tanaka, T. Togashi, K. Togawa, A. Tokuhisa, H. Tomizawa, K. Tono, S. Wu, M. Yabashi, M. Yamaga, A. Yamashita, K. Yanagida, C. Zhang, T. Shintake, H. Kitamura and N. Kumagai, *Nat. Photonics*, 2012, **6**, 540-544.
55. K. Tetsuo, H. Takashi, M. Yuki, S. Yasuhisa, O. Taito, O. Shigeki, T. Tadashi and Y. Makina, *J. Synchrotron Radiat.*, 2019, **26**, accepted.
56. S. Nozawa, S.-i. Adachi, J.-i. Takahashi, R. Tazaki, L. Guerin, M. Daimon, A. Tomita, T. Sato, M. Chollet, E. Collet, H. Cailleau, S. Yamamoto, K. Tsuchiya, T. Shioya, H. Sasaki, T. Mori, K. Ichiyanagi, H. Sawa, H. Kawata and S.-y. Koshihara, *J. Synchrotron Radiat.*, 2007, **14**, 313-319.
57. J. F. Marucco and A. Htiwech, *J. Solid State Chem.*, 1981, **40**, 197-202.
58. L. A. Bursill, *J. Solid State Chem.*, 1983, **48**, 256-271.
59. M. Gerosa, C. Di Valentin, G. Onida, C. E. Bottani and G. Pacchioni, *J. Phys. Chem. C*, 2016, **120**, 11716-11726.
60. F. Wang, C. Di Valentin and G. Pacchioni, *J. Phys. Chem. C*, 2012, **116**, 8901-8909.